Effective Treatment of Human Breast Carcinoma Xenografts with Single-Dose ^{211}At-Labeled Anti-HER2 Single-Domain Antibody Fragment

Yutian Feng, Rebecca Meshaw, Xiao-Guang Zhao, Stephen Jannetti, Ganesan Vaidyanathan, and Michael R. Zalutsky

Department of Radiology, Duke University Medical Center, Durham, North Carolina

Single-domain antibody fragments (sdAbs) are attractive for targeted α-particle therapy, particularly with ^{211}At, because of their rapid accumulation in tumor and clearance from normal tissues. Here, we evaluate the therapeutic potential of this strategy with 5F7 and VHH_1028—2 sdAbs that bind with high affinity to domain IV of human epidermal growth factor receptor type 2 (HER2). **Methods:** The HER2-specific sdAbs and HER2-irrelevant VHH_2001 were labeled using *N*-succinimidyl-3-^{211}At-astato-5-guanidinomethyl benzoate (*iso*-^{211}At-SAGMB). The cytotoxicity of *iso*-^{211}At-SAGMB-5F7 and *iso*-^{211}At-SAGMB-VHH_2001 were compared on HER2-expressing BT474 breast carcinoma cells. Three experiments in mice with subcutaneous BT474 xenografts were performed to evaluate the therapeutic effectiveness of single doses of *iso*-^{211}At-SAGMB-5F7 (0.7–3.0 MBq), *iso*-^{211}At-SAGMB-VHH_1028 (1.0–3.0 MBq), and *iso*-^{211}At-SAGMB-VHH_1028 and *iso*-^{211}At-SAGMB-VHH_2001 (~1.0 MBq). **Results:** Clonogenic survival of BT474 cells was reduced after exposure to *iso*-^{211}At-SAGMB-5F7 (D_0 = 1.313 kBq/mL) whereas *iso*-^{211}At-SAGMB-VHH_2001 was ineffective. Dose-dependent tumor growth inhibition was observed with ^{211}At-labeled HER2-specific 5F7 and VHH_1028 but not with HER2-irrelevant VHH_2001. At the 3.0-MBq dose, complete tumor regression was seen in 3 of 4 mice treated with *iso*-^{211}At-SAGMB-5F7 and 8 of 11 mice treated with *iso*-^{211}At-SAGMB-VHH_1028; prolongation in median survival was 495% and 414%, respectively. **Conclusion:** Combining rapidly internalizing, high-affinity HER2-targeted sdAbs with the *iso*-^{211}At-SAGMB residualizing prosthetic agent is a promising strategy for targeted α-particle therapy of HER2-expressing cancers.

Key Words: single-domain antibody fragment; α-emitter; radiopharmaceutical therapy; ^{211}At, HER2; nanobody

J Nucl Med 2023; 64:124–130
DOI: 10.2967/jnumed.122.264071

The human epidermal growth factor receptor type 2 (HER2) is overexpressed on breast, ovarian, and gastric cancers (*1*) and frequently is associated with metastatic progression (*2*). Although HER2-targeted therapies can improve survival, resistance to these therapies often occurs (*3*). Moreover, these agents are ineffective against brain metastases, an increasingly prevalent and lethal consequence of HER2-positive breast cancer (*4*). For these reasons, targeted therapies with different mechanisms of action and suitable for delivery to disease within the brain are urgently needed.

Targeted α-particle therapy (TAT) has emerged as an attractive strategy for cancer treatment and exerts its cytotoxic effects through mechanisms (*5*) different from currently approved HER2-targeted drugs. Moreover, their 50- to 100-μm tissue range in combination with their high cytotoxicity make α-particles of promise for irradiation of metastases while minimizing toxicity to surrounding normal tissues. This provided motivation for labeling HER2-targeted antibodies with a variety of α-emitters and evaluating their therapeutic potential in animal models (*6–9*) and in patients (*10*). Although some encouraging results were reported, the large size of intact antibodies led to slow and inhomogeneous delivery to tumor and prolonged residence time in normal tissues (*11*).

To circumvent these limitations, single-domain antibody fragments (sdAbs; aka nanobodies or VHH) are being evaluated as an alternative scaffold for TAT, with HER2 being perhaps the most widely investigated molecular target (*11,12*). Derived from camelids, these 12- to 15-kDa proteins can have nanomolar or subnanomolar affinity and exhibit low immunogenicity (*13*). Importantly, preclinical studies have demonstrated the considerably more rapid tumor penetration of sdAbs compared with intact antibodies (*14*) as well as their successful delivery to HER2-positive brain tumors (*15*). The feasibility of labeling HER2 domain I targeted 2Rs15 d with the α-emitters ^{225}Ac (*16*) and ^{213}Bi (*17*) has been reported. Although tumor targeting was demonstrated, high renal uptake also was observed.

On the other hand, labeling this anti-HER2 sdAb with the α-emitting radiohalogen ^{211}At resulted in much more favorable tumor-to-kidney ratios (*18*). Moreover, ^{211}At has a half-life (7.2 h) that is well-matched to the pharmacokinetics of sdAbs in humans (*19*). ^{211}At has other attractive features for TAT including emitting only 1 α-particle per decay, lack of confounding α-particle recoil effects, and increasing availability at a reasonable cost (*20*).

Our previous studies have shown that synergizing the characteristics of the ^{211}At-labeled prosthetic agent and the anti-HER2 sdAb can provide excellent tumor targeting (*21*). Herein, we evaluate the therapeutic efficacy of these ^{211}At-labeled sdAb conjugates and demonstrate a durable dose-dependent therapeutic effect after a single dose in a subcutaneous breast carcinoma xenograft model.

MATERIALS AND METHODS

General

Details about general procedures including cell culture and the sources for materials used in these experiments are presented in the supplemental materials (available at http://jnm.snmjournals.org) (*20,22,23*).

Received Mar. 1, 2022; revision accepted May 25, 2022.
For correspondence or reprints, contact Michael R. Zalutsky (zalut001@mc.duke.edu).
Published online May 26, 2022.

sdAbs

The characteristics of the anti-HER2 sdAbs 5F7 and VHH_1028, both reacting with the trastuzumab HER2 binding site, have been described previously (*24,25*). A HER2-irrelevant control, VHH_2001, was constructed by combining the framework amino acid sequences of these anti-HER2 sdAbs (same for both) with the CDR sequences from green fluorescent protein (GFP)–specific sdAb cAbGFP4 (*26*). All sdAbs were produced by ATUM using their known amino acid sequences as described (*25*).

Radiosynthesis and Quality Control of Iso-^{211}At-SAGMB-sdAb Conjugates

The synthesis of *iso*-^{211}At-SAGMB was modified for higher ^{211}At radioactivity level labeling based on a previously published method (*21*). ^{211}At in *N*-chlorosuccinimide/methanol (~370 MBq) was added to a vial containing 150 μg of Boc_2-SGMTB precursor followed by 4 μL of acetic acid. The reaction mixture was vortexed and incubated at room temperature for 30 min. Methanol was evaporated with a gentle stream of nitrogen; to ensure its complete removal, addition of 100 μL of ethyl acetate and its evaporation was performed twice. The residue was reconstituted with 100 μL of 30% (v/v) ethyl acetate in hexanes, and Boc_2-*iso*-^{211}At-SAGMB was isolated by normal-phase high-performance liquid chromatography (HPLC) (two 50-μL injections). For both runs, the HPLC fractions containing Boc_2-*iso*-^{211}At-SAGMB were pooled and the solvents were evaporated under a stream of argon. Boc-protecting groups were removed by treatment of each reaction vial with 100 μL of trifluoroacetic acid at room temperature for 10 min. To ensure complete removal of trifluoroacetic acid, ethyl acetate addition (100 μL) and its evaporation was performed 3 times. A solution of the sdAb (5F7, VHH_1028, or VHH_2001) in 0.1 M borate buffer (pH = 8.5, 50 μL, 2 mg/mL) was added to the vial containing *iso*-^{211}At-SAGMB, and the mixture was incubated at room temperature for 20 min. *Iso*-^{211}At-SAGMB-sdAb conjugates were purified by gel filtration using a PD-10 column eluted with phosphate-buffered saline (PBS) as described (*21*).

The *iso*-^{211}At-SAGMB-sdAbs were evaluated by SDS-PAGE (sodium dodecyl sulfate–polyacrylamide gel electrophoresis) and in some cases gel-permeation HPLC (GPC) as described in the supplemental materials. Target binding fractions were determined using HER2-coated beads (*24*) but following a modified procedure recently developed (*27*). The HER2 binding affinities of therapeutic batches of *iso*-^{211}At-SAGMB-5F7 and *iso*-^{211}At-SAGMB-VHH_1028 were determined on BT474 cells as described previously (*23*).

In Vitro Experiments

Cell Uptake and Internalization Kinetics. The internalization rate constant (k_e) and the washout rate constant (k_x) for *iso*-^{211}At-SAGMB-5F7 were determined as reported previously (*28*). Briefly, BT474 cells (8×10^5 cells/well/3 mL of medium) in 6-well plates were incubated overnight at 37°C. Medium was removed and replenished with fresh medium containing 1 nmol of *iso*-^{211}At-SAGMB-5F7, and the fraction of unbound, surface-bound, and internalized ^{211}At activity after incubation at 37°C for 1, 2, 3, 4, 5, and 6 h was determined as described (*23,24*). Nonspecific binding, determined in parallel by coincubation with a 100-fold molar excess of trastuzumab, was minimal. A similar format was used to determine the washout rate constant k_x by measuring the loss of internalized ^{211}At activity as a function of time. The internalization process was assumed to be linear, and the internalization rate constant k_e was expressed as $k_e \times t_{in} = m_i/m_b$, where t_{in} is the incubation time, m_i is the internalized fraction, and m_b is the surface-bound fraction. Rate constants were then calculated as described (*28*).

Cell Survival Assay. The cytotoxicity of *iso*-^{211}At-SAGMB-5F7 and HER2-unreactive *iso*-^{211}At-SAGMB-VHH_2001 were compared on BT474 cells in a colony-forming assay as described in the supplemental materials (*29*).

In Vivo Experiments

Animal Procedures. Animal studies conformed to protocols approved by the Duke University Animal Care and Use Committee for compliance with the National Institutes of Health for use of laboratory animals.

Biodistribution. Four-week-old female athymic mice (25 g; Jackson Labs) received subcutaneous implants of estrogen pellets (17β-estradiol, 0.72 mg) in the neck. Subcutaneous BT474 xenografts were established 2 d later by shoulder inoculation of 20×10^6 BT474 cells in 1:1 (v/v) Matrigel (100 μL, Matrigel Matrix; Corning) in tissue culture medium (100 μL). When tumors reached approximately 250 mm^3, animals received *iso*-^{211}At-SAGMB-VHH_1028 (200 kBq/1 μg, 100 μL of PBS) via intravenous injection. Groups of 5 mice were killed by isoflurane overdose at 1, 4, and 21 h after injection and necropsied. Tumor and normal tissues were harvested and counted for ^{211}At activity using an automated γ-counter. Results were expressed as percentage injected dose (%ID) per organ and per gram of tissue (%ID/g). The biodistribution of HER2-irrelevant *iso*-^{211}At-SAGMB-VHH_2001 (130 kBq/1 μg) was evaluated in the same way. Finally, a paired-label study directly compared the tissue distribution of *iso*-^{125}I-SGMIB-5F7 and *iso*-^{131}I-SGMIB-VHH_1028 in athymic mice bearing subcutaneous HER2-expressing SKOV-3 xenografts generated as described (*25*). Animals received approximately 175 kBq (1 μg) of both radioiodinated anti-HER2 sdAbs, and groups of 5 mice were necropsied at 1, 4, and 24 h after injection. For each animal, the ^{131}I-to-^{125}I tumor uptake ratio was determined, and differences in *iso*-^{131}I-SGMIB-VHH_1028 and *iso*-^{125}I-SGMIB-5F7 tumor accumulation were analyzed for statistical significance using a paired *t* test.

Radiation Dosimetry. From the *iso*-^{211}At-SAGMB-VHH_1028 biodistribution data, areas under the time–activity curves were calculated by trapezoidal integration using GraphPad Prism (GraphPad Software). These were multiplied by the mean energy per ^{211}At transition (4×10^{-13} Gy kg/Bq s) and ^{211}Po daughter (1.2×10^{-12} Gy kg/Bq s), corrected for the branching ratio. The absorbed dose was calculated using a radiation weighting factor of 5 for α-particles as recommended (*30*) and expressed as Sv/MBq.

Antitumor Efficacy. In the first experiment (Supplemental Table 1), the therapeutic efficacy of *iso*-^{211}At-SAGMB-5F7 was evaluated in NOD-*scid*-IL2Rgamma^{null} (NSG; Jackson Labs) mice with subcutaneous BT474 xenografts generated as described previously (*23*). Tumor growth was monitored twice a week, and tumor volume was calculated as volume = length × width^2 × 0.52. When tumor volumes reached 150–300 mm^3, mice were randomized into 4 groups and injected intravenously with PBS ($n = 10$) or 0.7 ($n = 4$), 1.9 ($n = 6$), or 3 MBq ($n = 4$) of *iso*-^{211}At-SAGMB-5F7 (3–14 μg of sdAb). Animals were monitored for 182 d as described in the last paragraph of this section.

In the second experiment (Supplemental Table 2), groups of 10–12 female athymic mice with approximately 180 mm^3 subcutaneous BT474 xenografts generated as described for the first experiment were injected intravenously with 1, 1.9, or 3 MBq of *iso*-^{211}At-SAGMB-VHH_1028 in 100 μL of PBS or PBS alone and monitored for 205 d.

In the third experiment (Supplemental Table 3), the specificity of the therapeutic effect was investigated in female athymic mice bearing BT474 xenografts. After estrogen pellet implantation (17β-estradiol, 0.72 mg), mice were supplied with ascorbic acid (240 mg/L) and citric acid (1 g/L) in their drinking water to prevent urolithiasis. Mice with approximately 120 mm^3 tumors were randomized into 3 groups, and injected intravenously with 1.0 MBq of *iso*-^{211}At-SAGMB-VHH_1028 ($n = 11$, 3 μg), 1.1 MBq of *iso*-^{211}At-SAGMB-VHH_2001 ($n = 11$, 3.7 μg), or PBS ($n = 10$). Animals were monitored for 196 d.

In these experiments, mice were euthanized if any of the following occurred: tumor volume > 1,000 mm^3, body weight loss > 20%, tumor

ulceration or necrosis, or any other health conditions that necessitated euthanasia per Duke Institutional Animal Care and Use Committee policy. Deceased animals were necropsied to determine cause of death.

Statistics

Data are presented as mean ± SD. Methods for statistical and data analysis of the therapeutic efficacy studies ae described in the supplemental materials.

RESULTS

Radiosynthesis and Quality Control of Iso-^{211}At-SAGMB-sdAb Conjugates

In previous studies performed with 30–56 MBq ^{211}At activity, Boc_2-*iso*-^{211}At-SAGMB was synthesized with 66.8% ± 2.4% average yield in ~4 h (*21*). The procedure was optimized for reactions with approximately 370 MBq of ^{211}At by varying the reaction volume, reaction time, acetic acid level, and normal-phase HPLC column injection volume. The Boc_2-*iso*-^{211}At-SAGMB radiochemical yield (RCY) was lower for reactions with approximately 370 MBq of ^{211}At (31.0% ± 7.1% [$n = 10$]); the radiochemical purity (RCP) determined by normal-phase HPLC was greater than 99%. Deprotection of Boc_2-*iso*-^{211}At-SAGMB to generate *iso*-^{211}At-SAGMB was almost quantitative, with a maximum of 222 MBq of *iso*-^{211}At-SAGMB being produced. Conjugation of *iso*-^{211}At-SAGMB to sdAbs proceeded in 51.9% ± 14.7% ($n = 9$) RCY with no significant differences observed among 5F7, VHH_1028, and VHH_2001. The total synthesis time for producing these *iso*-^{211}At-SAGMB-sdAb conjugates from initial ^{211}At activity was 3.5 h, with an overall RCY of 16.1% ± 7.0%. A typical synthesis starting from 370 MBq of ^{211}At provided approximately 74 MBq of ^{211}At-labeled sdAb. The molar activity for the *iso*-^{211}At-SAGMB-sdAbs was 1.74–4.41 MBq/nmole.

SDS-PAGE/phosphor imaging of the *iso*-^{211}At-SAGMB-sdAbs revealed a single radioactive band corresponding to the expected molecular weight of approximately 13 kDa (Supplemental Fig. 1), with an RCP of 97.6% ± 0.8% ($n = 9$). The RCP of 4 batches of *iso*-^{211}At-SAGMB-VHH_1028 also was evaluated by GPC-HPLC (Supplemental Fig. 2), which indicated a single peak at the expected retention time and an RCP of 98.6% ± 1.0%. The target binding fraction was 84.3% ($n = 2$) for *iso*-^{211}At-SAGMB-5F7 and 87.1% ($n = 1$) for *iso*-^{211}At-SAGMB-VHH_1028. No HER2 binding was observed for the HER2-irrelevant *iso*-^{211}At-SAGMB-VHH_2001 control. Saturation binding assays on HER2-expressing BT474 breast cancer cells performed with therapy-level batches of *iso*-^{211}At-SAGMB-5F7 and *iso*-^{211}At-SAGMB-VHH_1028 gave K_D values of 4.49 ± 0.39 and 3.87 ± 0.88 nM, respectively (Supplemental Fig. 3).

In Vitro Experiments

Internalization and Expulsion Rate. To quantify the rate of internalization of *iso*-^{211}At-SAGMB-5F7, the ratio between internalized and surface-bound ^{211}At activity was plotted as a function of incubation time (Supplemental Fig. 4). A linear regression was run to give $k_e = (3.79 \pm 0.29) \times 10^{-5}$ (s^{-1}) (95% CI: $R^2 = 0.9155$). The rate constant for ^{211}At loss (expulsion; k_x) was determined in similar fashion based on a washout kinetics assay. Expulsion of radioactivity was not observed during the 4-h experimental period as the ratio of m_i/m_b increased; thus, k_x was considered to be 0.

Cell Survival Assay. The survival fraction of HER2-positive BT474 breast carcinoma cells after incubation with varying activity concentrations of *iso*-^{211}At-SAGMB-5F7 prepared at 3.9 MBq/nmole is given in Figure 1. The D_0 (activity concentration to reduce survival to 37%) was determined to be 1.313 kBq/mL for *iso*-^{211}At-SAGMB-5F7. The cytotoxicity of the *iso*-^{211}At-SAGMB-VHH_2001 control was measured in parallel, and no reduction in survival was observed (Fig. 1), demonstrating that the cytotoxicity of *iso*-^{211}At-SAGMB-5F7 was HER2-specific.

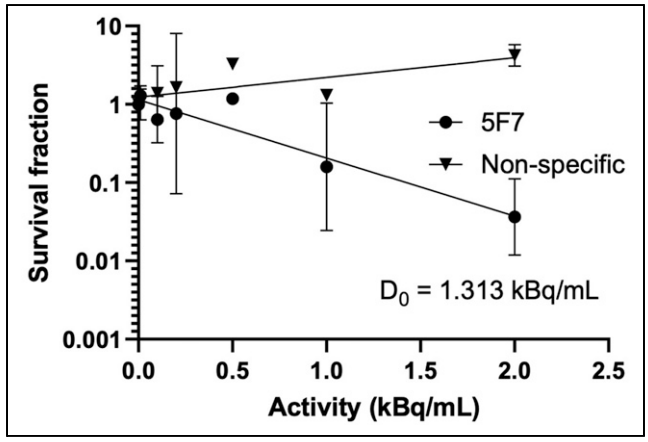

FIGURE 1. Survival fraction of BT474 breast carcinoma cells after incubation with *iso*-^{211}At-SAGMB-5F7 and HER2-irrelevant *iso*-^{211}At-SAGMB-VHH_2001.

In Vivo Experiments

Biodistribution and Dosimetry. The tissue distribution of *iso*-^{131}I-SGMIB-VHH_1028 in NSG mice with BT474 xenografts was reported previously (*21*). The biodistribution of *iso*-^{211}At-SAGMB-VHH_1028 in athymic mice with subcutaneous BT474 xenografts is summarized in Figure 2. The tumor uptake of *iso*-^{211}At-SAGMB-VHH_1028 was 10.28 ± 0.90 %ID/g at 1 h and 10.21 ± 3.10 %ID/g at 4 h and decreased to 4.00 ± 1.90 %ID/g at 21 h. Rapid clearance of radioactivity from normal organs was observed. The highest ^{211}At levels were seen in the kidneys, decreasing from 34.20 ± 13.63 %ID/g at 1 h to 4.46 ± 0.62 %ID/g at 4 h. Thyroid activity levels ranged from 0.53% ± 0.25% at 4 h to 0.38% ± 0.17% at 21 h (Supplemental Table 4) consistent with only minor dehalogenation in vivo. Tumor uptake of HER2-irrelevant *iso*-^{211}At-SAGMB-VHH_2001 was 3.17 ± 0.50 %ID/g, 2.05 ± 0.23 %ID/g, and

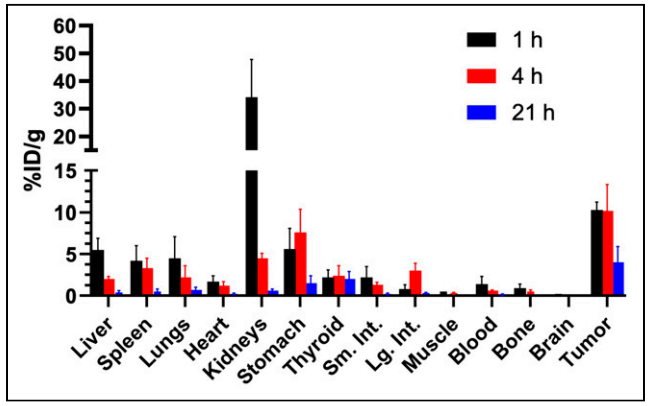

FIGURE 2. Biodistribution of *iso*-^{211}At-SAGMB-VHH_1028 in athymic mice with subcutaneous BT474 xenografts. Sm. Int. = small intestine; Lg. Int. = large intestine.

TABLE 1
Estimated Absorbed Doses for *iso*-^{211}At-SAGMB-VHH_1028 in Athymic Mice with Subcutaneous BT474 Xenografts

Tissue	Absorbed dose (Sv/1.0 MBq)	Absorbed dose (Sv/3.0 MBq)
Liver	3.8	11.3
Spleen	4.8	14.3
Lungs	3.7	11.2
Heart	1.8	5.4
Kidneys	14.6	43.7
Stomach	9.9	29.7
Thyroid	3.5	10.6
Small intestine	2.0	6.1
Large intestine	3.5	10.4
Muscle	0.5	1.4
Blood	1.1	3.2
Bone	0.8	2.4
Brain	0.2	0.5
Tumor	14.4	43.3

0.58 ± 0.58 %ID/g (Supplemental Table 5) at 1, 4, and 21 h, respectively, values 3.2, 5.0, and 7.7 times lower than those for *iso*-^{211}At-SAGMB-VHH_1028. The biodistribution of coadministered *iso*-^{131}I-SGMIB-VHH_1028 and *iso*-^{125}I-SGMIB-5F7 in athymic mice with SKOV-3 xenografts is summarized in Supplemental Table 6. With few exceptions, normal-tissue levels for the 2 sdAbs were not significantly different. In tumor, ^{131}I-to-^{125}I uptake ratios were not significantly different from unity (1.07 ± 0.20 at 1 h, 0.99 ± 0.01 at 4 h, and 0.91 ± 0.10 at 24 h) confirming equivalent tumor localizing capacity for the 5F7 and VHH_1028 *iso*-SGMIB conjugates.

Radiation-absorbed doses calculated from the *iso*-^{211}At-SAGMB-VHH_1028 biodistribution data are presented in Table 1 both per MBq and for 3.0 MBq, the highest ^{211}At activity evaluated in the therapeutic efficacy experiments. The tumor absorbed dose was estimated to be 14.4 Sv/MBq, which was higher than that calculated for all normal tissues except the kidneys (14.6 Sv/MBq). At 3.0 MBq, the tumor was estimated to have received a radiation dose of 43.3 Sv. The tumor absorbed dose for *iso*-^{211}At-SAGMB-VHH_2001 was estimated to be 3.08 Sv/MBq, 4.7 times lower than that for *iso*-^{211}At-SAGMB-VHH_1028.

Antitumor Efficacy. The first experiment evaluated the therapeutic potential of *iso*-^{211}At-SAGMB-5F7 in NSG mice with BT474 xenografts; tumor volumes at treatment and dosing details are summarized in Supplemental Table 1. A dose-dependent tumor growth delay was observed (Fig. 3A)—tumor growth was significantly delayed for the 3.0-MBq group ($P < 0.0001$), to a degree that was significantly greater than in the 1.9-MBq ($P = 0.0001$) and 0.7-MBq ($P < 0.0001$) groups. A maximum tumor growth inhibition of > 50% was observed in 1 of 4 mice in the 0.7-MBq group, 5 of 6 in the 1.9-MBq group, and all 4 in the 3.0-MBq group, both the 1.9- and the 3.0-MBq groups having 3 mice with no detectable tumors (Fig. 3B). A significant survival benefit was seen for the treatment groups ($P < 0.0001$), with a median survival of 29 d for the control group, and 105.5, 126.5, and 143.5 d for the 0.7-, 1.9-, and 3.0-MBq groups, respectively (Fig. 3C). No significant differences in body weight (Fig. 3D) or other clinically observable signs of toxicity were seen between the treatment and control groups.

Tumor volumes at treatment and dosing details for the single-dose *iso*-^{211}At-SAGMB-VHH_1028 therapy study in athymic mice with BT474 xenografts are summarized in Supplemental Table 2. Significant tumor growth delay was observed in all treatment groups ($P < 0.0001$), which was dose-dependent ($P = 0.0011$ for 3.0- vs. 1.9-MBq doses; $P < 0.0001$ for 3.0- vs. 1.0-MBq doses) (Fig. 4A). However, the therapeutic responses were not significantly different for the 1.0- versus 1.9-MBq doses. A single dose of *iso*-^{211}At-SAGMB-VHH_1028 resulted in the complete regression of tumors in 8 of 11 mice receiving 3.0 MBq, 3 of 12 mice receiving 1.9 MBq, and 3 of 10 mice receiving 1.0 MBq, with > 50% tumor volume regression seen in 11 of 11, 10 of 12, and 7 of 10 animals receiving the 3.0-, 1.9-, and 1.0-MBq doses, respectively (Fig. 4B). A significant survival benefit ($P < 0.0001$ from Mantel–Cox and Gehan–Breslow–Wilcoxon tests) was observed for all treatment groups. A single dose of *iso*-^{211}At-SAGMB-VHH_1028 increased the median survival from 50.5 d (control group) to 209 d (3.0-MBq group) (Fig. 4C). No significant differences in body weight (Fig. 4D) or other clinically observable signs of toxicity were seen between the treatment and control groups.

The third therapy study was designed to evaluate the specificity of the *iso*-^{211}At-SAGMB-VHH_1028 therapeutic effect by direct comparison to the HER2-unreactive *iso*-^{211}At-SAGMB-VHH_2001 control. A Spaghetti plot of individual mouse tumor volumes (Fig. 5A) and a waterfall plot of maximum tumor response (Fig. 5B) indicate significant tumor growth delay for the HER2-specific *iso*-^{211}At-SAGMB-sdAb conjugate, with 6 of 11 mice showing > 50% tumor regression and 4 mice showing no evidence of tumor at the 1.0-MBq dose. In contrast, no tumor growth delay was seen in

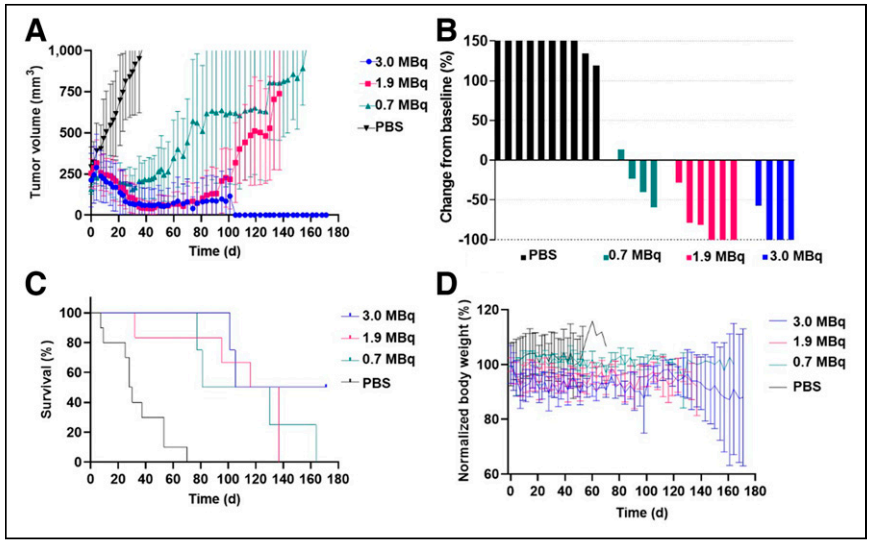

FIGURE 3. Therapeutic efficacy of single-dose *iso*-^{211}At-SAGMB-5F7 in NSG mice with BT474 xenografts. (A) Tumor volume. (B) Maximum tumor response waterfall plot. (C) Kaplan–Meier curve. (D) Normalized body weight.

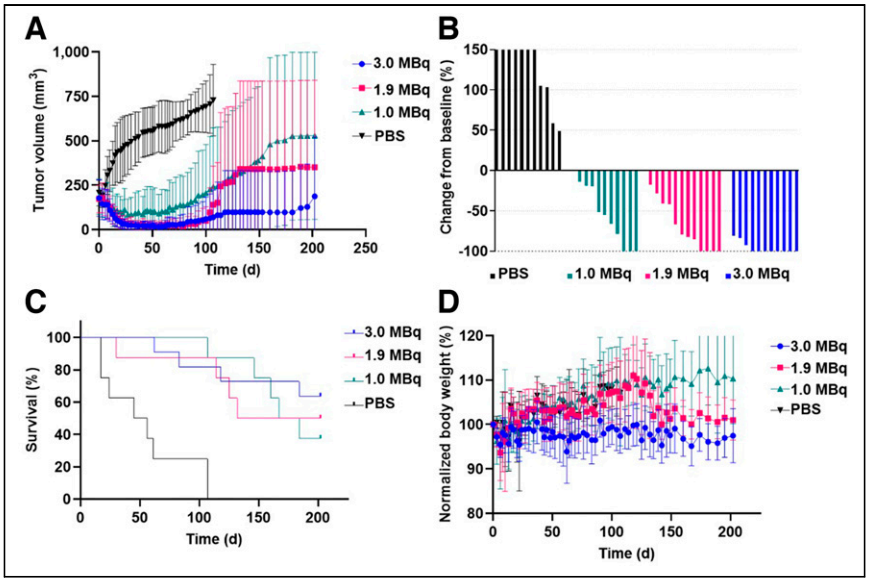

FIGURE 4. Therapeutic efficacy of single-dose *iso*-^{211}At-SAGMB-VHH_1028 in athymic mice with BT474 xenografts. (A) Tumor volume. (B) Maximum tumor response waterfall plot. (C) Kaplan–Meier curve. (D) Normalized body weight.

animals receiving the *iso*-^{211}At-SAGMB-sdAb control. As shown in Figure 5C, no significant difference was observed between the median survival of the PBS group (44 d) and the *iso*-^{211}At-SAGMB-sdAb control (34 d). A clear survival benefit was seen for the HER2-specific *iso*-^{211}At-SAGMB-VHH_1028 conjugate, with a median survival of 159 versus 44 d for the PBS group ($P < 0.0001$; Mantel–Cox and Gehan-Breslow-Wilcoxon tests). No significant differences in body weight (Fig. 5D) or other clinically observable signs of toxicity were seen between the treatment and control groups.

DISCUSSION

Because of their rapid and homogeneous tumor penetration (*14*), sdAbs have emerged as an attractive vehicle for TAT (*12*). In the present study, we have demonstrated that dramatic tumor control could be achieved in a HER2-expressing subcutaneous model of breast cancer after a single-dose of ^{211}At-labeled HER2-targeted sdAbs. ^{211}At is ideally suited for labeling sdAbs because its 7.2-h half-life is well matched to the approximately 8-h biologic clearance half-life of labeled sdAbs in humans (*19*). Moreover, in studies where the same sdAb was labeled with different α-emitters, kidney activity levels were considerably lower for ^{211}At (*18*) than ^{213}Bi (*17*) and ^{225}Ac (*16*), suggesting that an additional benefit in selecting ^{211}At for labeling sdAbs is the lower risk of renal toxicity. Other more generalizable advantages of ^{211}At for TAT include the emission of only 1 α-particle per decay, absence of α-emitting daughters, and improved availability at a reasonable cost (*20*).

Herein, we have evaluated a TAT development strategy for HER2-expressing cancers, combining the best currently available ^{211}At residualizing agent—*iso*-^{211}At-SAGMB (*21*)—with HER2-specific sdAbs with high affinity and internalization, properties that should enhance and prolong tumor uptake of these small proteins (*31*). For anti-HER2 sdAbs, initial studies used 5F7, which has a HER2 binding affinity of 0.2 nM (*32*) and exhibited excellent uptake in BT474 cells and xenografts after being labeled with *iso*-^{211}At-SAGMB (*21*). VHH_1028 also binds to a trastuzumab-competitive HER2 site with 0.2 nM affinity (*25*). A head-to-head comparison using ^{131}I-SGMIB-5F7 and ^{131}I-SGMIB-VHH_1028 confirmed that the 2 sdAbs cross compete for the same HER2 epitope and bind to BT474 cells with nearly identical characteristics (Supplemental Fig. 5).

The binding affinities determined on BT474 cells for *iso*-^{211}At-SAGMB-5F7 and *iso*-^{211}At-SAGMB-VHH_1028 were 4.49 ± 0.39 and 3.87 ± 0.88 nM, respectively. The *iso*-^{211}At-SAGMB-5F7 affinity was somewhat higher than measured previously (3.0 nM) at lower ^{211}At activities (*21*) but still suitable for TAT. Regarding internalization, the internalization rate and lack of measurable expulsion of *iso*-^{211}At-SAGMB-5F7 were in excellent agreement with those measured previously on BT474 cells for trastuzumab (*28*). Thus, the cellular residence time for *iso*-^{211}At-SAGMB-5F7 should be compatible with effective cell killing. Indeed, the cytotoxicity of *iso*-^{211}At-SAGMB-5F7 ($D_0 = 1.313$ kBq/mL) was higher than that determined for ^{211}At-trastuzumab (1.7 kBq/mL) under similar conditions on the same BT474 cell line (*28*).

Therapeutic responses after ^{211}At-trastuzumab treatment have been observed in various animal models; however, except for a recent study (*33*), these have involved direct delivery into a tumor-compromised compartment (*6,34*). After intrathecal delivery, regional differences in therapeutic effectiveness against carcinomatous meningitis were

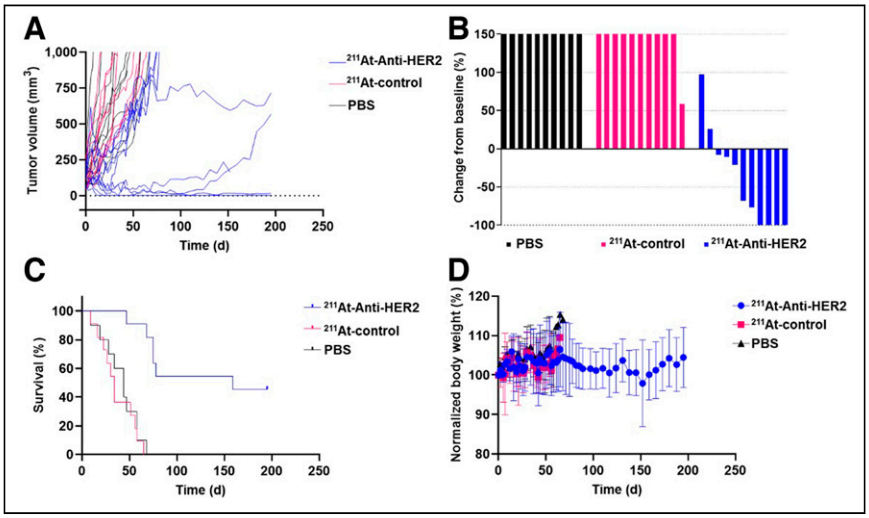

FIGURE 5. Therapeutic efficacy of single-dose *iso*-^{211}At-SAGMB-VHH_1028 and HER2-irrelevant *iso*-^{211}At-SAGMB-VHH_2001 in athymic mice with BT474 xenografts. (A) Tumor volume in individual mice. (B) Maximum tumor response waterfall plot. (C) Kaplan–Meier curve. (D) Normalized body weight.

observed with ^{211}At-trasuzumab, suggesting that inhomogeneous distribution of the labeled mAb had occurred (*6*). In addition, a recent study has demonstrated that unlike trastuzumab, sdAbs can be delivered to HER2-positive brain metastases (*35*), for which better treatments are urgently needed (*4*). Thus, a ^{211}At-labeled sdAb with trastuzumablike binding and internalization properties but capable of more homogeneous delivery might be advantageous, provided that the delivery of therapeutically relevant levels to tumor could be achieved.

On the basis of the biodistribution of *iso*-^{211}At-SAGMB-VHH_1028 in athymic mice, a tumor dose of 14.4 Sv/MBq was calculated, which is higher than that reported (4.58 Gy/MBq) for ^{211}At-trastuzumab in a gastric cancer–liver metastases model (*33*). We note that the BT474 tumor targeting (and kidney uptake) of *iso*-^{211}At-SAGMB-VHH_1028 determined in athymic mice were lower than those reported previously for *iso*-^{211}At-SAGMB-5F7 in NSG mice bearing the same xenograft (*21*). Given the similar properties of the 2 VHH, this behavior likely reflects animal model–dependent differences in distribution. Consistent with this, the BT474 tumor and kidney uptake of *iso*-^{131}I-SGMIB-5F7 were lower in athymic mice (*32,36*) than in NSG mice (*21*). An additional experiment was performed to confirm that differences in the biodistribution of *iso*-^{211}At-SAGMB-5F7 and *iso*-^{211}At-SAGMB-VHH_1028 reflected the influence of the mouse strain. A paired-label study in athymic mice bearing HER2-expressing SKOV-3 xenografts demonstrated essentially identical tumor uptake of *iso*-^{125}I-SGMIB-5F7 and *iso*-^{131}I-SGMIB-VHH_1028 (Supplemental Table 6).

Although different animal models and sdAbs were used, the therapeutic efficacy of other α-emitter–anti-HER2 sdAb conjugates has been evaluated and can serve as benchmarks for comparison. Using an intracranial SKOV3.IP1 ovarian tumor model, 3 weekly doses of ^{225}Ac-2Rs15 d increased median survival by 35% (6 d) (*35*). Administration of 3 doses of ^{213}Bi-2Rs15 d to mice with intraperitoneal SKOV3.IP1 tumors increased median survival by 51% and 26% at doses of 0.5 and 1.0 MBq, respectively (*17*). Although gelofusine was coadministered to reduce renal retention, the kidney radiation dose from ^{213}Bi-2Rs15 d was 6 times higher than that to tumor (*17*), likely limiting dose escalation.

The therapeutic responses we observed after a single dose of *iso*-^{211}At-SAGMB-VHH_1028 in the BT474 breast carcinoma model are thus quite encouraging. Notably, even at the lowest dose level investigated (1.0 MBq), median survival was increased by 361%, from 44 d to 159 d (Fig. 5C), with 4 of 11 animals having complete tumor regression, whereas no significant survival prolongation was observed with the HER2-irrelevant ^{211}At-sdAb control. Importantly, these responses were obtained at ^{211}At activity that would deliver only 14.6 Sv to the kidneys (Table 1). Although radiation toxicity thresholds for TAT are not well defined, this dose is well below the 23-Gy benchmark threshold for renal toxicity for conventional external beam radiation, for which 1 Gy = 1 Sv. Finally, these results further confirm the potential advantages of TAT for cancer treatment—a single dose of *iso*-^{211}At-SAGMB-VHH_1028 was considerably more effective than 4 weekly doses of the analogous β-emitting *iso*-^{131}I-SGMIB-VHH_1028 conjugate in the same BT474 xenograft model (*25*).

Because VHH_1028 lacks the CDR2 lysine present in 5F7, VHH_1028 might be better suited for patient therapy–level labeling. However, a recent study using surface plasmon resonance analysis demonstrated full retention of affinity for 1:1 *iso*-SGMIB-5F7 conjugate (K_D = 0.21 vs. 0.22 nM for unmodified 5F7 run in parallel) (*36*), suggesting that either the CDR2 lysine was not reactive for conjugation or its modification did not alter HER2 binding. With ^{211}At at a 1:1 prosthetic agent:5F7 substitution level, this would be equivalent to 1,221 GBq/mg. Even if the protein dose for an ^{211}At-5F7 therapy was limited to 50 μg, the dose administered to patients in a recent ^{131}I-labeled anti-HER2 sdAb imaging study (*19*), this would be equivalent to 61 GBq (~1,650 mCi) of ^{211}At, an activity level far exceeding a feasible patient therapy dose. Thus, the CDR2 lysine in 5F7 should not compromise ^{211}At labeling at therapeutically relevant activities, suggesting that both 5F7 and VHH_1028 are excellent candidates for development as ^{211}At-labeled radiopharmaceuticals for treating HER2-expressing cancers.

A limitation of this study is that it did not include histopathologic analysis of acute and long-term radiotoxicity and determination of the maximum tolerated dose. Given the lack of clinically observable toxicities at the highest dose investigated and a median survival greater than 6 mo, it might be possible to achieve even better single-dose tumor response at a higher activity level. A long-term radiotoxicity study is planned that will include histopathologic analysis and evaluation of blood chemistry as we have done for other ^{211}At-labeled TAT agents (*37*). This will provide critical information for designing future dose escalation experiments and, it is hoped, for clinical translation of these *iso*-^{211}At-SAGMB-targeted sdAb conjugates.

CONCLUSION

TAT with single doses of *iso*-^{211}At-SAGMB-anti-HER2-sdAb conjugates resulted in significant tumor growth delay and survival prolongation in a murine model of HER2-expressing breast cancer with no apparent normal-tissue toxicities. This TAT strategy warrants further consideration for the treatment of patients with HER2-expressing cancers.

DISCLOSURE

Financial support was received from NIH grant CA42324 and Cereius, Inc. Ganesan Vaidyanathan and Michael Zalutsky are shareholders in Cereius and are entitled to royalty distributions from Cereius related to the radiolabeling technologies described herein. No other potential conflict of interest relevant to this article was reported.

KEY POINTS

QUESTION: Are ^{211}At-labeled sdAb conjugates candidates for targeted α-particle therapy of HER2-expressing cancers?

PERTINENT FINIDINGS: ^{211}At-labeled sdAbs targeting domain IV of HER2 controlled tumor growth and prolonged survival at single doses of 0.7–3.0 MBq without toxicity, whereas a ^{211}At-labeled HER2-irrelevant sdAb was ineffective.

IMPLICATIONS FOR PATIENT CARE: Because of their considerable therapeutic effects with minimal normal-tissue toxicity, these *iso*-^{211}At-SAGMB-sdAb conjugates could provide an attractive therapeutic option for patients who do not respond to conventional HER2-targeted therapies.

REFERENCES

1. Oh D-Y, Bang Y-J. HER2-targeted therapies—a role beyond breast cancer. *Nat Rev Clin Oncol.* 2020;17:33–48.

2. Slamon DJ, Leyland-Jones B, Shak S, et al. Use of chemotherapy plus a monoclonal antibody against HER2 for metastatic breast cancer that overexpresses HER2. *N Engl J Med.* 2001;344:783–792.
3. Pernas S, Tolaney SM. HER2-positive breast cancer: new therapeutic frontiers and overcoming resistance. *Ther Adv Med Oncol.* 2019;11:1758835919833519.
4. Hosonaga M, Saya H, Arima Y. Molecular and cellular mechanisms underlying brain metastasis of breast cancer. *Cancer Metastasis Rev.* 2020;39:711–720.
5. Pouget J-P, Constanzo J. Revisiting the radiobiology of targeted alpha therapy. *Front Med (Lausanne).* 2021;8:692436.
6. Boskovitz A, McLendon RE, Okamura T, Sampson JH, Bigner DD, Zalutsky MR. Treatment of HER2-positive breast carcinomatous meningitis with intrathecal administration of α-particle-emitting ^{211}At-labeled trastuzumab. *Nucl Med Biol.* 2009;36:659–669.
7. Milenic DE, Garmestani K, Dadachova E, et al. Targeting of HER2 antigen for the treatment of disseminated peritoneal disease. *Clin Cancer Res.* 2004;10:7834–7841.
8. Borchardt PE, Yuan RR, Miederer M, McDevitt MR, Scheinberg DA. Targeted actinium-225 in vivo generators for therapy of ovarian cancer. *Cancer Res.* 2003; 63:5084–5090.
9. Wickstroem K, Karlsson J, Ellingsen C, et al. Synergistic effect of a HER2 targeted thorium-227 conjugate in combination with Olaparib in a BRCA2 deficient xenograft model. *Pharmaceuticals (Basel).* 2019;12:155.
10. Meredith R, Torgue J, Shen S, et al. Dose escalation and dosimetry of first-in-human α radioimmunotherapy with ^{212}Pb-TCMC-trastuzumab. *J Nucl Med.* 2014; 55:1636–1642.
11. Altunay B, Morgenroth A, Beheshti M, et al. HER2-directed antibodies, affibodies and nanobodies as drug-delivery vehicles in breast cancer with a specific focus on radioimmunotherapy and radioimmunoimaging. *Eur J Nucl Med Mol Imaging.* 2021;48:1371–1389.
12. Dekempeneer Y, Keyaerts M, Krasniqi A, et al. Targeted alpha therapy using short-lived alpha-particles and the promise of nanobodies as targeting vehicle. *Expert Opin Biol Ther.* 2016;16:1035–1047.
13. Piramoon M, Khodadust F, Hosseinimehr SJ. Radiolabeled nanobodies for tumor targeting: from bioengineering to imaging and therapy. *Biochim Biophys Acta Rev Cancer.* 2021;1875:188529.
14. Debie P, Lafont C, Defrise M, et al. Size and affinity kinetics of nanobodies influence targeting and penetration of solid tumors. *J Control Release.* 2020;317:34–42.
15. Zhou Z, Vaidyanathan G, McDougald D, et al. Fluorine-18 labeling of the HER2-targeting single-domain antibody 2Rs15d using a residualizing label and preclinical evaluation. *Mol Imaging Biol.* 2017;19:867–877.
16. Pruszynski M, D'Huyvetter M, Bruchertseifer F, Morgenstern A, Lahoutte T. Evaluation of an antiHER2 nanobody labeled with ^{225}Ac for targeted α-particle therapy of cancer. *Mol Pharm.* 2018;15:1457–1466.
17. Dekempeneer Y, Caveliers V, Ooms M, et al. Therapeutic efficacy of ^{213}Bi-labeled sdAbs in a preclinical model of ovarian cancer. *Mol Pharm.* 2020;17:3553–3566.
18. Dekempeneer Y, Back T, Aneheim E, et al. Labeling of anti-HER2 nanobodies with astatine-211: optimization and the effect of different coupling reagents on their *in vivo* behavior. *Mol Pharm.* 2019;16:3524–3533.
19. D'Huyvetter M, Vos J, Caveliers V, et al. Phase I trial of ^{131}I-GMIB-Anti-HER2-VHH1, a new promising candidate for HER2-targeted radionuclide therapy in breast cancer patients. *J Nucl Med.* 2021;62:1097–1105.
20. Feng Y, Zalutsky MR. Production, purification and availability of ^{211}At: near term steps towards global access. *Nucl Med Biol.* 2021;100-101:12–23.
21. Choi J, Vaidyanathan G, Koumarianou E, Kang CM, Zalutsky MR. Astatine-211 labeled anti-HER2 5F7 single domain antibody fragment conjugates: Radiolabeling and preliminary evaluation. *Nucl Med Biol.* 2018;56:10–20.
22. Pozzi OR, Zalutsky MR. Radiopharmaceutical chemistry of targeted radiotherapeutics III: part 3: α-particle-induced radiolytic effects on the chemical behavior of ^{211}At. *J Nucl Med.* 2007;48:1190–1196.
23. Pruszynski M, Koumarianou E, Vaidynathan G, et al. Improved tumor targeting of anti-HER2 nanobody through *N*-succinimidyl 4-guanidinomethyl-3-benzoate radiolabelling. *J Nucl Med.* 2014;55:650–656.
24. Pruszynski M, Koumarianou E, Vaidynathan G, et al. Targeting breast carcinoma with radioiodinated antiHER2 nanobody. *Nucl Med Biol.* 2013;40:52–59.
25. Feng Y, Meshaw R, McDougald D, et al. Evaluation of an ^{131}I-labeled HER2-specific single domain antibody fragment for the radiopharmaceutical therapy of HER2-expressing cancers. *Sci Rep.* 2022;12:3020.
26. Saerens D, Pellis M, Loris R, et al. Identification of a universal VHH framework to graft non-canonical antigen-binding loops of camel single-domain antibodies. *J Mol Biol.* 2005;352:597–607.
27. Sharma SK, Lyashchenko SK, Park HA, et al. A rapid bead-based radioligand binding assay for the determination of target-binding fraction and quality control of radiopharmaceuticals. *Nucl Med Biol.* 2019;71:32–38.
28. Akabani G, Carlin S, Welsh P, Zalutsky MR. In vitro cytotoxicity of ^{211}At-labeled trastuzumab in human breast cancer cell lines: effect of specific activity and HER2 receptor heterogeneity on survival fraction. *Nucl Med Biol.* 2006;33:333–347.
29. Kiess AP, Minn I, Vaidyanathan G, et al. (2S)-2-(3-(1-carboxy-5-(4-^{211}At-astatobenzamido)pentyl)ureido)-pentanedioic acid for PSMA-targeted α-particle radiopharmaceutical therapy. *J Nucl Med.* 2016;57:1569–1575.
30. Sgouros G, Roeske JC, McDevitt MR, et al. MIRD pamphlet no. 22: radiobiology and dosimetry of alpha-particle emitters for targeted radionuclide therapy. *J Nucl Med.* 2010;51:311–328.
31. Schmidt MM, Wittrup KD. A modeling analysis of the effects of molecular size and binding affinity on tumor targeting. *Mol Cancer Ther.* 2009;8:2861–2871.
32. Zhou Z, Meshaw R, Zalutsky MR, Vaidyanathan G. Site-specific and residualizing linker for ^{18}F labeling with enhanced renal clearance: application to anti-HER2 single-domain antibody fragment. *J Nucl Med.* 2021;62:1624–1630.
33. Li HK, Morokoshi Y, Kodaira S, et al. Utility of ^{211}At-trastuzumab for the treatment of metastatic gastric cancer in the liver: evaluation of a preclinical α-radioimmunotherapy approach in a clinically relevant mouse model. *J Nucl Med.* 2021;62: 1468–1474.
34. Palm S, Back T, Claesson I, et al. Therapeutic efficacy of astatine-211-labeled trastuzumab on radioresistant SKOV-3 tumors in nude mice. *Int J Radiat Oncol Biol Phys.* 2007;69:572–579.
35. Puttemans J, Dekempeneer Y, Eersels JL, et al. Preclinical targeted α- and β-radionuclide therapy in HER2-positive brain metastasis using camelid single-domain antibodies. *Cancers (Basel).* 2020;12:1017.
36. Feng Y, Zhou Z, McDougald D, Meshaw RL, Vaidyanathan G, Zalutsky MR. Site-specific radioiodination of an anti-HER2 single domain antibody fragment with a residualizing prosthetic agent. *Nucl Med Biol.* 2021;92:171–183.
37. Mease RC, Kang CM, Kumar V, et al. An improved ^{211}At-labeled agent for PSMA-targeted α-therapy. *J Nucl Med.* 2022;63:259–267.